

Characterizing Error Mitigation by Symmetry Verification in QAOA

Ashish Kakkar^{✉*}, Jeffrey Larson^{✉†}, Alexey Galda^{✉‡}, and Ruslan Shaydulin^{✉†}

^{*}Dept. of Physics and Astronomy, University of Kentucky, Lexington, KY, USA

[†]Mathematics and Computer Science, Argonne National Laboratory, Lemont, IL, USA

[‡] Menten AI, Inc., San Francisco, CA, USA

Email: ^{*}ashish.kakkar@uky.edu, [†]{jmlarson,rshaydulin}@anl.gov, [‡]alexey.galda@menten.ai

Abstract—Hardware errors are a major obstacle to demonstrating quantum advantage with the quantum approximate optimization algorithm (QAOA). Recently, symmetry verification has been proposed and empirically demonstrated to boost the quantum state fidelity, the expected solution quality, and the success probability of QAOA on a superconducting quantum processor. Symmetry verification uses parity checks that leverage the symmetries of the objective function to be optimized. We develop a theoretical framework for analyzing this approach under local noise and derive explicit formulas for fidelity improvements on problems with global \mathbb{Z}_2 symmetry. We numerically investigate the symmetry verification on the MaxCut problem and identify the error regimes in which this approach improves the QAOA objective. We observe that these regimes correspond to the error rates present in near-term hardware. We further demonstrate the efficacy of symmetry verification on an IonQ trapped ion quantum processor where an improvement in the QAOA objective of up to 19.2% is observed.

Index Terms—quantum computing, error mitigation, quantum optimization, Quantum Approximate Optimization Algorithm, QAOA, trapped-ion quantum processor

I. INTRODUCTION

Quantum computers have the potential to demonstrate a computational advantage in the near term over state-of-the-art classical algorithms [1]. In the recent years, the size and the quality of quantum processors have increased [2] and their computational power has become competitive with that of classical supercomputers on certain tasks [3], [4]. However, near-term quantum devices are still characterized by high error rates that impose limits on their computational power. Although in the long term quantum error correction provides a solution to this problem [5], the currently available devices are far from satisfying the preconditions for error correction. This situation motivates the development of error mitigation techniques, which provide some degree of robustness to errors while avoiding the high overhead of full error correction.

The quantum approximate optimization algorithm (QAOA) is one of the most promising near-term algorithms with the possibility of showing a quantum advantage [6]–[8]. QAOA approximately solves a combinatorial optimization problem by preparing a parameterized quantum state. The parameters are chosen such that upon the measurement of the state, an approximate solution to the target problem is retrieved with high probability. These parameters are typically obtained by using some classical numerical optimization method. A major

motivation for the study of QAOA is the existence of worst-case performance bounds that are competitive with classical local search approximation algorithms [6], [9].

The presence of noise on current quantum devices has a drastic effect on the applicability of QAOA. Indeed, recent results demonstrate that under realistic noise assumptions and in the absence of error mitigation, QAOA cannot outperform even a simple classical competitor on modestly sized problems [10]. Moreover, recent studies [11], [12] show the effects of noise on QAOA parameters and the objective landscape: under local noise, the fidelity of the noisy state decays exponentially with the number of qubits, N , on the order of $(1-p)^N$, where p characterizes the error rate. Wang et al. [13] have noted that because of the effects of local noise, gradients of the QAOA objective with respect to QAOA parameters vanish while the general landscape does not change much. The vanishing of the gradients makes it harder to optimize the QAOA parameters. Therefore, error mitigation is a prerequisite for realizing the potential of QAOA.

Many error mitigation strategies have been proposed for near-term quantum devices [14]. Improving the estimate of the expectation of some observable is the goal of several recently proposed techniques. These include zero-noise extrapolation [15], [16], probabilistic error cancellation [17], and virtual distillation [18]. Quantum subspace expansion [19] uses classical postprocessing to remove the overhead of explicitly performing parity checks on the hardware and decoding the errors from the measurement outcomes.

While just improving the estimate of the expectations of the observables is sufficient in some cases, often an improvement in the fidelity of the quantum state is also necessary. This is the problem we address in this work. The approach we consider is symmetry verification (SV), which was initially proposed for the variational quantum eigensolver [20], [21]. Symmetry verification mitigates hardware errors by performing parity checks based on the symmetries of the problem Hamiltonian and postselecting based on the measurement outcomes. For example, if the problem Hamiltonian H commutes with a given Pauli string P , we say that P is the symmetry of H . When studying H on a noisy quantum computer, we can restrict the quantum state evolution to one eigenspace of P . Then the value (“parity”) of P can be measured and the state postselected on the measurement outcome corresponding to

the that eigenspace of P .

It has been shown that symmetries of the classical objective function to be optimized are preserved by the QAOA ansatz [22]. These symmetries can therefore be verified by using parity checks, with the postselection enforcing the symmetry. This approach was applied to QAOA for the MaxCut problem and was demonstrated to improve the quantum state fidelity on a cloud-based superconducting IBM quantum processor [23].

In this work we provide analytical and numerical evidence for the power of symmetry verification to mitigate the errors in QAOA evolution when performed on a noisy quantum device. We begin by developing a theoretical framework for analyzing the fidelity improvements from symmetry verification under local noise. We use this framework to provide explicit formulas for the fidelity improvements in the limit of noise-free parity checks. We then analyze symmetry verification numerically under a more realistic noisy checks assumption, and we identify a regime in which the symmetry verification leads to QAOA objective improvements. This regime correspond to the error rates expected on near-term hardware. We verify the expected efficacy of symmetry verification on real quantum devices by performing experiments on IonQ trapped-ion processors and observing QAOA objective improvements of up to 19.2%.

The rest of the paper is organized as follows. Section II introduces QAOA, problem symmetries, symmetry verification, and our model for device noise. Section III considers the case of noise-free parity checks and local noise and presents analytical results on the fidelity improvement from symmetry verification. Section IV outlines the procedure for verifying permutation symmetries inherited from problem instances. Section V demonstrates QAOA objective improvements from symmetry verification numerically under a specific error model, with noise applied to both the QAOA circuit and the parity checks. Section VI presents the results obtained on IonQ trapped-ion quantum processors.

II. BACKGROUND

Consider the objective function $c(x)$. We study the problem of finding $x \in \{0, 1\}^N$ that maximizes c :

$$\max_{x \in \{0, 1\}^N} c(x). \quad (1)$$

Our results are general and apply to a wide range of objective functions with symmetries. The example problem we study numerically is MaxCut: Given a graph G with nodes V and edges E , find a partition of the nodes into two sets so that the number of edges between the sets is maximized. MaxCut on general graphs is APX-complete; that is, there does not exist a polynomial-time classical approximation algorithm for MaxCut unless $P = NP$ [24].

The classical objective function $c(x)$ on N bits is represented by a diagonal operator (Hamiltonian) in the computational basis as

$$H = \sum_{x \in \{0, 1\}^N} c(x) |x\rangle \langle x|. \quad (2)$$

For MaxCut problem instances, this is

$$H = \frac{1}{2} \sum_{(i,j) \in E} (I - Z_i Z_j), \quad (3)$$

where Z_i denotes the Pauli Z operator on the i th qubit and the identity operator on the rest of the qubits.

A. The quantum approximate optimization algorithm

QAOA approximately solves optimization problems by preparing a parameterized quantum state by acting on the initial state $|+\rangle^{\otimes N}$ with operators $U_B(\beta_i) = e^{-i\beta_i B}$ and $U_H(\gamma_i) = e^{-i\gamma_i H}$:

$$|\vec{\beta}, \vec{\gamma}\rangle_d = U_B(\beta_d)U_H(\gamma_d)\dots U_B(\beta_1)U_H(\gamma_1)|+\rangle^N. \quad (4)$$

The initial state $|+\rangle^{\otimes N}$ is the ground state of the operator $B = \sum_{j=1}^n X_j$. Typically, a classical numerical optimization method is used to identify parameters $\vec{\beta}, \vec{\gamma}$ that minimize the expectation value

$$\langle \vec{\beta}, \vec{\gamma} | H | \vec{\beta}, \vec{\gamma} \rangle_d. \quad (5)$$

We refer to the value of (5) as the ‘‘QAOA objective’’ or simply the ‘‘objective.’’ The approximation ratio for QAOA with a given set of $\vec{\beta}, \vec{\gamma}$ at depth d is defined as $\langle \vec{\beta}, \vec{\gamma} | H | \vec{\beta}, \vec{\gamma} \rangle_d / C_{\max}$, where $C_{\max} = \max_{x \in \{0, 1\}^N} c(x)$.

B. Symmetries in QAOA

A symmetry of the objective function $c(x)$ is a permutation acting on binary strings $s : x \rightarrow s(x)$ that leaves the objective unchanged, that is, $c(s(x)) = c(x) \forall x \in \{0, 1\}^N$. For MaxCut on a graph $G = (V, E)$, we consider two classes of symmetries. The first is the \mathbb{Z}_2 symmetry, which is present for any graph G and acts as a bit flip on x . The second class of symmetries we consider is problem instance specific. These symmetries are permutations of the indices of the bit string x , that is, $s \in S_N$. If a permutation s satisfies $(s(u), s(v)) \in E$ when $(u, v) \in E$, s is a symmetry of the MaxCut objective for G .

A transformation s that leaves the objective function invariant is represented on the N -qubit Hilbert space by the operator

$$S = |s(x_1)s(x_2)\dots s(x_N)\rangle \langle x_1x_2\dots x_N|. \quad (6)$$

In particular, the bit-flip symmetry operator is represented by

$$S_B = \prod_i X_i \quad \forall i \in V. \quad (7)$$

, and the permutation on two qubits (i, j) (i.e., the SWAP gate) is represented by

$$S_{i,j} = \frac{1}{2} (I_i \otimes I_j + X_i \otimes X_j + Y_i \otimes Y_j + Z_i \otimes Z_j). \quad (8)$$

QAOA preserves the symmetries of the objective function [22]. Concretely, Theorem 1 in [22] states that *the QAOA ansatz $|\vec{\beta}, \vec{\gamma}\rangle$ is stabilized by a symmetry operator S if $[S, B] = 0$, $[S, H] = 0$, and $S|+\rangle^{\otimes N} = |+\rangle^N$* . We will discuss arbitrary

permutation symmetries in Section IV; for now we focus on S_B and $S_{i,j}$. The initial state $|+\rangle^N$ is stabilized by S_B and arbitrary permutations, including $S_{i,j}$. Moreover, $[B, S_B] = 0 = [B, S_{i,j}]$ trivially. As a result, for any G , the MaxCut QAOA ansatz is stabilized by S_B . If G is invariant under the permutation of nodes (i, j) , then the corresponding ansatz is stabilized by $S_{i,j}$.

C. Symmetry verification

We now briefly review error mitigation by symmetry verification [20]. If the initial state is in the $+1$ eigenspace of a symmetry S , then in the absence of errors it must stay in this eigenspace during circuit evolution. If errors occur during the evolution, however, the state may not remain in the $+1$ eigenspace of S . Projective measurements of S can then be used to detect errors by checking whether the state is in the correct eigenspace after the noisy circuit evolution. To construct the set of projective measurement operators for the symmetry S , we consider its spectral decomposition. Because both S_B and $S_{i,j}$ satisfy $S^2 = I$, we can write

$$S = \sum_{s=\pm 1} sP_s, \quad (9)$$

where $P_s = \frac{1}{2}(I + sS)$ are projectors onto the eigenspace corresponding to eigenvalues $s = \pm 1$.

Let $|\psi\rangle\langle\psi|$ denote the (hypothetical) noise-free state prepared by the circuit, and let ρ_{noisy} denote the state with errors. A projective measurement of S is performed, and only measurements corresponding to the $+1$ eigenvalue are kept. The corresponding circuit is shown in Fig. 1. This is equivalent to the projector P_{+1} acting on the prepared state. This process has the following important effect: the postselected state $\rho_{\text{SV}} = \frac{P_{+1}\rho_{\text{noisy}}P_{+1}}{\text{Tr}(P_{+1}\rho_{\text{noisy}})}$ has a greater overlap with the error-free state $|\psi\rangle\langle\psi|$. This overlap is captured by the fidelity of the state after SV, denoted by F_{SV} :

$$F_{\text{SV}} = \text{Tr}(\rho_{\text{SV}}|\psi\rangle\langle\psi|) = \frac{\text{Tr}(\rho_{\text{noisy}}|\psi\rangle\langle\psi|)}{\text{Tr}(P_{+1}\rho_{\text{noisy}})}. \quad (10)$$

Noting that the fidelity of the noisy state without error mitigation is $F_{\text{noisy}} = \text{Tr}(\rho_{\text{noisy}}|\psi\rangle\langle\psi|)$, we can write the ratio

$$\frac{F_{\text{SV}}}{F_{\text{noisy}}} = \frac{1}{\text{Tr}(P_{+1}\rho_{\text{noisy}})}. \quad (11)$$

This ratio is a measure of the improvement in the fidelity of the postselected state due to symmetry verification. We denote F_{SV} by F_{S_B} when the symmetry being verified is S_B and by $F_{S_{i,j}}$ if the symmetry is $S_{i,j}$.

D. Modeling the errors in QAOA

For our theoretical analysis we model the noise occurring in the QAOA evolution as local (single-qubit) error channels. Specifically, we follow a commonly used error model that applies a layer of a single-qubit noise channel after each pair of QAOA operators (i.e., a ‘‘QAOA layer’’) [11]–[13]. We study the physically relevant depolarizing and dephasing noise channels. Let $\rho = |\psi\rangle\langle\psi|$ denote the (noiseless) pure state

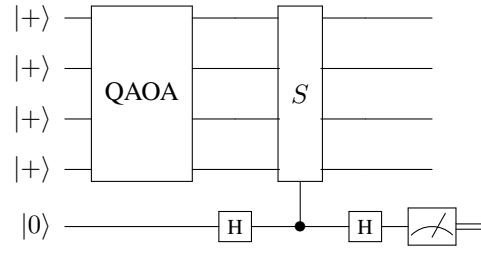


Fig. 1: Verification of symmetry S on the QAOA state. Postselecting on the ancilla measurement outcome 0 projects the state $|\psi\rangle$ to $P_{+1}|\psi\rangle$.

prepared by a single layer of QAOA. Our model assumes this state is acted upon by the noise channel \mathcal{E}_i on the i^{th} qubit.

The single-qubit depolarizing noise channel is defined by the set of Kraus operators $E_a \in \{\sqrt{(1-p)}I, \sqrt{\frac{p}{3}}X, \sqrt{\frac{p}{3}}Y, \sqrt{\frac{p}{3}}Z\}$ and acts on ρ as

$$\mathcal{E}_i(\rho) = (1-p)I\rho I + \left(\frac{p}{3}X_i\rho X_i + \frac{p}{3}Y_i\rho Y_i + \frac{p}{3}Z_i\rho Z_i\right). \quad (12)$$

We additionally consider the single-qubit dephasing noise channel acting as

$$\mathcal{E}_i(\rho) = (1-p)I\rho I + (pZ_i\rho Z_i). \quad (13)$$

Here $p \leq 1$, and the normalizations are chosen to ensure that the map is trace preserving, namely, $\sum_a E_a^\dagger E_a = I$.

These single-qubit noise channels act on all qubits, with the state after a single layer of QAOA given by

$$\rho_1 = \mathcal{E}(\rho) = \prod_{i=1}^N \mathcal{E}_i(\rho), \quad (14)$$

where each \mathcal{E}_i acts independently. Note that only the noise operator \mathcal{E} factorizes over qubits; the state ρ is a general N -qubit state. The noise channel is then applied repeatedly after each QAOA layer. We can generalize to d layers of QAOA by writing the action of each QAOA layer (indexed by t) as $\mathcal{U}^{(t)}(\beta_t, \gamma_t)$ and the noise channel between each layer as $\mathcal{E} = \prod_{i=1}^N \mathcal{E}_i$. We arrive at the following density matrix for the noisy state at depth d :

$$\rho_d = \mathcal{E} \circ \mathcal{U}^{(d)} \circ \dots \circ \mathcal{E} \circ \mathcal{U}^{(1)} \circ (|+\rangle^{\otimes N} \langle +|^{\otimes N}). \quad (15)$$

A high-level overview of the noise model is given in Fig. 2 with SV performed after the final layer.

III. MITIGATING THE EFFECTS OF LOCAL NOISE ON QAOA

Recent results [10]–[12], [23] show that using error mitigation strategies to minimize the effects of local noise is necessary in order to achieve quantum advantage with QAOA. Here we demonstrate that error mitigation via symmetry verification improves the fidelity of the QAOA state under local noise. We provide explicit formulas for the relationship between the fidelity improvement, probability of local noise, and circuit depth and size. Our formulas rely on the assumption that no noise is present during the decoding procedure (i.e., the

parity checks of symmetries are noiseless). In Section V we numerically investigate the fidelity improvements from symmetry verification with noisy parity checks.

A. Errors that commute with checks cannot be detected

When performing a parity check with a symmetry S , not every error E can be detected. If an error E commutes with S , then a check using S cannot detect it. The reason is that the action of E on the noise-free state $|\psi\rangle\langle\psi|$ keeps it within the symmetry-stabilized subspace: $P_{+1}E|\psi\rangle = EP_{+1}|\psi\rangle = E|\psi\rangle$. Therefore, to quantify the performance of SV with a symmetry S , we need to count the errors that commute with the symmetry.

To this end we use a convenient binary symplectic notation [25]. In this notation an arbitrary tensor product of Pauli operators and identity operators O is written in terms of length N binary vectors $\vec{\alpha}, \vec{\beta}$:

$$O = O(\alpha, \beta) = i^{\alpha \cdot \beta} (X^{\alpha_1} \otimes \dots \otimes X^{\alpha_N}) (Z^{\beta_1} \otimes \dots \otimes Z^{\beta_N}).$$

In particular, the symmetry $S_B = \prod_i X_i$ is $\alpha = \vec{1}, \beta = \vec{0}$.

The advantage of this notation is that the commutation relation can be written as

$$[O(\alpha, \beta), O'(\alpha', \beta')] = 0$$

if and only if

$$\alpha \cdot \beta' - \alpha' \cdot \beta \equiv 0 \pmod{2}.$$

The set of errors $O(\alpha, \beta)$ that commute with S_B can now be described by the set of α, β that satisfy

$$\alpha \cdot \vec{0} - \vec{1} \cdot \beta = -\vec{1} \cdot \beta \equiv 0 \pmod{2}. \quad (16)$$

The solution to this equation is the set of β with an even number of 1 as entries and α being an arbitrary binary vector.

B. Warm-up: one QAOA layer with one local error

We first consider the case where only a single error occurs after a single layer of QAOA. This highlights our point about undetectable errors and allows us to understand the relative advantage gained by verifying S_B and $S_{i,j}$. Let E_a be the error acting on a^{th} qubit. Because $|\psi\rangle$ is stabilized by S_B and $S_{i,j}$ and E_a either commute or anticommute, the following identities hold:

$$\langle\psi| E_a^\dagger S_B E_a |\psi\rangle = \begin{cases} 1 & \text{for } [E_a, S_B] = 0, \\ -1 & \text{for } \{E_a, S_B\} = 0. \end{cases} \quad (17)$$

The ratio of fidelities (11) is straightforward to calculate for the depolarizing error channel (12):

$$\frac{F_{S_B}}{F_{\text{noisy}}} = \frac{1}{\text{Tr}(P_{+1}\mathcal{E}(\rho))} = \frac{1}{\sum_a \langle\psi| E_a^\dagger \frac{(I+S)}{2} E_a |\psi\rangle} = \frac{1}{1 - \frac{2p}{3}}. \quad (18)$$

Let us compare this with symmetry verification by a single permutation on the two qubits i, j . We must look at the set of errors E_a that commute with the symmetry $S_{i,j}$. Unlike S_B , $S_{i,j}$ is not in the Pauli group, so it is no longer necessarily true that it only commutes or anticommutes with the errors

under consideration. However, for the cases $E_a = X_i, Y_i, Z_i$, respectively, we observe the following:

$$\langle\psi| E_a S_{i,j} E_a |\psi\rangle = \begin{cases} \frac{1}{2} \langle\psi| (I_i I_j + X_i X_j - Y_i Y_j - Z_i Z_j) |\psi\rangle \\ \frac{1}{2} \langle\psi| (I_i I_j - X_i X_j + Y_i Y_j - Z_i Z_j) |\psi\rangle \\ \frac{1}{2} \langle\psi| (I_i I_j - X_i X_j - Y_i Y_j + Z_i Z_j) |\psi\rangle \end{cases}$$

Notice the following useful identity:

$$\langle\psi| X_i S_{i,j} X_i |\psi\rangle + \langle\psi| Y_i S_{i,j} Y_i |\psi\rangle + \langle\psi| Z_i S_{i,j} Z_i |\psi\rangle = 1.$$

Assume that the depolarizing noise channel (12) acts on qubit i , followed by SV with the symmetry $S_{i,j}$. Then we can write

$$\frac{F_{S_{i,j}}}{F_{\text{noisy}}} = \frac{1}{\text{Tr}(P_{+1}\mathcal{E}_i(\rho))} = \frac{1}{\sum_a \langle\psi| E_a^\dagger \frac{(I+S)}{2} E_a |\psi\rangle} = \frac{1}{1 - \frac{p}{3}}. \quad (19)$$

Comparing (18) with (19) suggests that the bit-flip parity check is more effective than the permutation parity check on two qubits in detecting depolarizing errors on a single qubit. This provides an intuition for why we expect permutation symmetries to be less powerful in mitigating errors, an effect that has been observed numerically in simulation and on superconducting qubit hardware [23].

C. One QAOA layer with the full error model

We now analyze the improvement in fidelity from bit-flip symmetry verification under local noise acting on all qubits. We begin with the single-layer case given by (14) and then generalize to an arbitrary number of layers d . The goal is to understand the scaling behavior of the fidelity of the postselected state with number of qubits N and depth d , for a given probability of error p .

To calculate the improvement in fidelity from verifying a given symmetry (11), we need to find the expectation $\text{Tr}(P_{+1}\mathcal{E}(\rho))$. Only undetectable errors (those that commute with S_B) contribute. We begin with the cases of depolarizing noise and dephasing noise for depth $d = 1$.

1) *Depolarizing noise:* Let $K_{j_i}^{N_i}$ denote the Kraus operator labeled by j_i , which acts as the identity operator on all qubits except N_i . In particular, for depolarizing noise, the operators $K_1^{N_i}, K_2^{N_i}, K_3^{N_i}$ are $X_{N_i}, Y_{N_i}, Z_{N_i}$, respectively.

We follow the discussion in [12] and label the noisy state by the number of error operators m that have acted on it:

$$|\psi\rangle_{\text{noisy}}^m = \sum_{\vec{N}_m, \vec{j}_m} \psi_{\vec{j}_m}^{\vec{N}_m} = \sum_{\vec{N}_m, \vec{j}_m} K_{j_1}^{N_1} \dots K_{j_m}^{N_m} |\psi\rangle, \quad (20)$$

where \vec{N}_m, \vec{j}_m are length m vectors. Up to N single-qubit errors can occur. To find the action of the noise channel, we sum the probabilities of errors occurring on m qubits at a time:

$$\mathcal{E}(\rho) = \sum_{m=0}^N (1-p)^{N-m} \left(\frac{p}{3}\right)^m |\psi\rangle_{\text{noisy}}^m \langle\psi|_{\text{noisy}}^m. \quad (21)$$

Inserting the projector onto the +1 eigenspace yields

$$\text{Tr}(P_{+1}\mathcal{E}(\rho)) = \sum_{m=0}^N (1-p)^{N-m} \left(\frac{p}{3}\right)^m \langle\psi|_{\text{noisy}}^m \frac{1}{2} (I+S) |\psi\rangle_{\text{noisy}}^m.$$

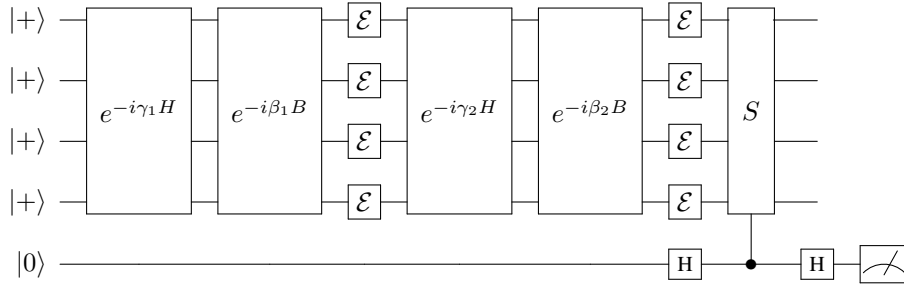


Fig. 2: Error model of local noise acting between each layer of QAOA followed by verification of symmetry S . \mathcal{E} is a noise channel that acts on each qubit locally.

Whenever $[S_B, K_{j_1}^{N_1} \dots K_{j_m}^{N_m}] = 0$, the contribution from matrix element $\langle \psi |_{\text{noisy}}^m \frac{1}{2} (I + S) | \psi \rangle_{\text{noisy}}^m$ is one; and when they anticommute, it is zero.

To count the nonzero contributions, we rewrite the sum as

$$\sum_{m=0}^N (1-p)^{N-m} \left(\frac{p}{3}\right)^m f(m), \quad (22)$$

where $f(m)$ counts the number of operators that commute with S_B . In our analysis of undetectable errors (16), these operators are described by pairs of length N binary vectors (α, β) such that α is arbitrary and $\beta \cdot \vec{1} \equiv 0 \pmod{2}$. Counting

the number of such vectors $f(m)$ is a problem that we solve in Appendix A. The result is

$$\begin{aligned} f(m) &= \frac{1}{2} \binom{N}{m} (1 + 3^m) \text{ for } m \text{ even.} \\ &= \frac{1}{2} \binom{N}{m} (-1 + 3^m) \text{ for } m \text{ odd,} \end{aligned}$$

$f(m)$ yields the ratio of fidelities for depolarizing noise at a depth $d = 1$:

$$\frac{F_{S_B}}{F_{\text{noisy}}} = \frac{1}{\sum_{m=0}^N (1-p)^{N-m} \left(\frac{p}{3}\right)^m f(m)} = \frac{1}{\mathcal{F}(N, p)}, \quad (23)$$

where

$$\begin{aligned} \mathcal{F}(N, p) &= \frac{1}{4} \left(1 + (1-2p)^N + \left(1 - \frac{4p}{3}\right)^N + \left(1 - \frac{2p}{3}\right)^N \right) + \frac{1}{4} (1-p)^{1+N} (-1+p)^{-1-N} \\ &\quad \left(-1 + (1-2p)^N + (-1+p)^N \left(1 - \frac{p}{3(-1+p)}\right)^N - (-1+p)^N \left(1 + \frac{p}{3(-1+p)}\right)^N \right). \end{aligned}$$

2) *Dephasing channel noise*: We now consider the case of depth $d = 1$ with the dephasing noise channel described by (13) acting on each qubit. Similar to the previous case, the expectation value takes the form

$$\text{Tr}(P_{+1} \mathcal{E}(\rho)) = \sum_{m=0}^N (1-p)^{N-m} (p)^m f(m). \quad (24)$$

The crucial difference is in the nonzero contribution to $f(m)$ in the evaluation of $[S_B, K_{j_1}^{N_1} \dots K_{j_m}^{N_m}]$. The errors are purely Z errors at multiple sites. In the binary symplectic notation, tensor products of Z operators satisfy $\vec{\alpha} = \vec{0}$. Thus, the only contribution to the sum arises from errors with $\vec{\alpha} = \vec{0}$ and $\vec{\beta}$ satisfying $\vec{\beta} \cdot \vec{1} \equiv 0 \pmod{2}$. The number of such errors is given by $f(m) = \binom{N}{m}$, where m is constrained to be even.

The ratio can be computed as follows:

$$\frac{F_{S_B}}{F_{\text{noisy}}} = \frac{1}{\sum_{m \text{ even}}^N (1-p)^{N-m} p^m f(m)} = \frac{2}{(1 + (1-2p)^N)}. \quad (25)$$

3) *Arbitrary depth d* : We now extend our results to a higher depth d under the full noise channel described by (15). Similar to the simpler $d = 1$ case, the errors that are not detected commute with S_B . One still needs only to compute the ratio

$$\frac{(F_{S_B})_d}{(F_{\text{noisy}})_d} = \frac{1}{\text{Tr}(P_{+1} \rho_d)}. \quad (26)$$

The noisy state $|\psi\rangle_{\text{noisy}}^m$ can be described by

$$|\psi\rangle_{\text{noisy}}^m = \sum_{\vec{N}_m, \vec{J}_m} \psi_{\vec{J}_m}^{\vec{N}_m} = \sum_{\vec{N}_m, \vec{J}_m} K_{j_1}^{N_1} \dots K_{j_m}^{N_m} |\psi\rangle,$$

where the length of the vector \vec{N}_m can be at most Nd instead of N because the error could have occurred at Nd locations.

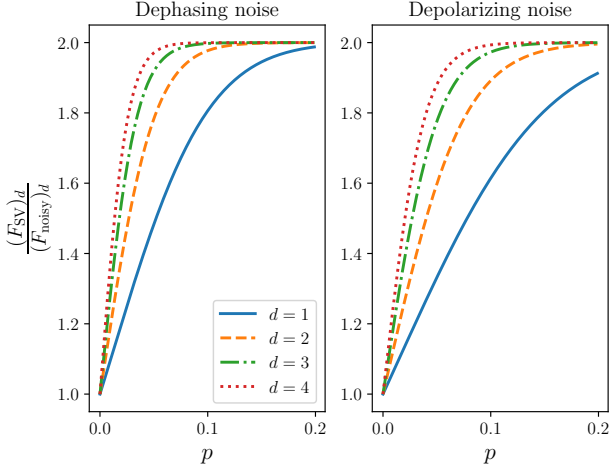


Fig. 3: Ratio of fidelities with and without SV for fixed $N = 10$ for varying depth. The value on the y axis is produced by Equations (27) and (28), which are based on the local noise model depicted in Fig. 2.

Because we assume that the noise channel factorizes over qubits and the channel acting on each qubit and depth is identical, ρ_d is effectively calculated by replacing $N \rightarrow Nd$ in the result, as is done in [12, Eq. (16)]. The end result is

$$\frac{(F_{S_B})_d}{(F_{\text{noisy}})_d} = \frac{1}{\sum_{m \text{ even}}^{Nd} (1-p)^{Nd-m} p^m f(m)} \approx \frac{2}{(1 + (1-2p)^{Nd})}. \quad (27)$$

For the depolarizing noise channel, a similar analysis gives

$$\frac{(F_{S_B})_d}{(F_{\text{noisy}})_d} \approx \frac{1}{\mathcal{F}(Nd, p)}, \quad (28)$$

4) *Qualitative observations:* The ratios of fidelities for depolarizing and dephasing error channels are plotted in Fig. 3 and have interesting features. First, for a fixed error rate p and fixed N , the fidelity boost provided by SV increases with the depth d . This increase is because there is a larger probability for a number of detectable errors to have accumulated in the circuit.

A second important feature is that for fixed values of p and d , $\frac{(F_{S_B})_d}{(F_{\text{noisy}})_d}$ saturates to 2 as $N \rightarrow \infty$. This suggests that in its current form, error mitigation with SV is not scalable to large N because the cost of applying the parity check via N CNOT gates scales linearly with N , while the fidelity boost saturates.

IV. VERIFYING HIGHER-ORDER PERMUTATION SYMMETRIES

In Section II problem-instance-specific permutation the symmetries were defined. We now address the question of whether verifying these symmetries for a given problem instance can give a significant fidelity boost.

To address this question, we must first calculate the projection operator onto the symmetry-stabilized subspace. Every

permutation of a finite set can be written as a cyclical permutation (cycle) or as a product of disjoint cycles. Constructing a set of orthogonal and complete projectors for each cycle is straightforward because each cycle s of length q must satisfy $s^q = 1$. The operator representing s on qubits satisfies $S^q = I$. As a result, the eigenvalues of this operator lie on the unit circle and are given by $e^{2\pi i \frac{k}{q}}$, where $k \in \{0, \dots, q-1\}$. The symmetry-stabilized subspace corresponds to the $k=0$ case, which is the subspace corresponding to the $+1$ eigenvalue.

To find the projector onto the $+1$ eigenspace of S , we factorize the following equation:

$$S^q - I = (\Phi_q(S))(S - I) = 0. \quad (29)$$

$\Phi_q(x)$ is the cyclotomic polynomial, which is the unique divisor of the polynomial equation $x^q - 1$. These polynomials are known in closed form. The final result is that $\Phi_q(S)$ projects vectors onto the $+1$ eigenspace of S .

To illustrate this point, we consider the permutation on three elements, denoted by the cycle $(1, 2, 3)$. This satisfies $s^3 - 1 = (1 + s + s^2)(s - 1) = 0$. The associated operator S can be implemented by successive SWAPS $S = \text{SWAP}_{1,2} \cdot \text{SWAP}_{2,3}$, and the projector onto the $+1$ eigenspace is

$$P_{+1} = \frac{1}{3} (I + S + S^2). \quad (30)$$

To see that (30) is correct, consider applying P_{+1} on any state $|v\rangle$ in the subspace associated with the eigenvalues $e^{2\pi i \frac{1}{3}}, e^{2\pi i \frac{2}{3}}$. Then $P_{+1}|v\rangle = 0$. This is because $(1 + s + s^2) = 0$ for $s = e^{2\pi i \frac{1}{3}}, e^{2\pi i \frac{2}{3}}$. The normalization is chosen to ensure that the corresponding eigenvalue is 1.

To construct the projector circuit, we define the shifted operator

$$U = \frac{1}{3} (2S + 2S^2 - I). \quad (31)$$

This operator is defined so that applying controlled- U and then postselecting the $+1$ eigenvalue projects onto the symmetry-stabilized subspace. Operator U is not trivial to decompose into gates in general. For simple cases like the example considered above, circuit synthesis tools such as QSearch [26] can be used.

For general cycles, however, the corresponding projector is difficult to decompose into gates. In this case, $(\Phi_q(S))$ gives an expression for the projector as a linear sum of permutation operators. One may leverage the techniques for implementing linear combinations of unitaries outlined in [27].

In general, for a given symmetry this task of projection onto the $+1$ eigenspace can be done by performing quantum phase estimation (QPE) and postselecting on the measurement outcome 0^N , which corresponds to measuring out eigenvalue $+1$. The resulting postselected state would be the state projected into the $+1$ eigenspace. Of course, using QPE for error mitigation is impractical. The high gate cost of QPE is due to the need to apply S, S^2, \dots, S^{2^k} , controlled on the ancilla qubit, where k is the number of binary digits sufficient to distinguish the $+1$ eigenvalue with some target probability.

Symmetry verification of higher-order permutations may be beneficial, but without further advances it may not be viable because of the high overhead of performing the symmetry checks. One promising direction is generalizing the efficient postprocessing methods that do not rely on directly verifying the symmetries using projectors, such as those developed in [28] for symmetries with generators in the Pauli group.

V. EXPERIMENTS IN SIMULATION

In this section we present the results from numerical simulations of symmetry verification. We assign error rates to all single- and two-qubit gates, including those used to perform the parity checks. The circuit is first decomposed into a set of native single-qubit gates R_x , R_y , and R_z and the two-qubit gate CNOT. The following error channel acts every time a gate is applied, with $k = 1, 2$ for single- and two-qubit gates, respectively:

$$\mathcal{E}(\rho) = (1 - p_k) \rho + p_k \frac{\text{Tr}(\rho)}{2^n} I. \quad (32)$$

The error rates associated with single-qubit gate fidelities are typically smaller than those of two-qubit gate fidelities by an order of magnitude on common hardware platforms [29], [30]. To model this, we set $p_1 = \frac{1}{10} p_2$.

We use preoptimized QAOA parameters from noiseless simulations because the noise model we use does not affect the value of optimal QAOA parameters [11], [13]. For depth $d \leq 3$ we use parameters available in QAOAKit [31], and for $d > 3$ we find them by using exhaustive numerical optimization.

To quantify the effect of errors on the QAOA circuit, we consider the expectation value of the cost function in the noisy state $\langle H \rangle$ given by (5). Our results are presented in Fig. 4. We consider random regular graphs with number of nodes $N \in \{8, 10, \dots, 18\}$, degree $\in \{3, 4, 5, 6\}$, and depth $d \in \{1, 2, 3, 4, 5, 6\}$. To map out the space of error rates where SV shows an improvement, we consider the following quality measure of improvement after symmetry verification:

$$R = \frac{\langle H \rangle_{\text{SV}}}{\langle H \rangle_{\text{no-SV}}} - 1. \quad (33)$$

When $R > 0$, we see an improvement in fidelity by applying SV (indicated by the color blue in Fig. 4).

For each degree and number of nodes, we observe a clear regime of error rates and circuit depths in which symmetry verification leads to improvements in the QAOA objective. We see that this regime corresponds to realistic error rates that can be expected on near-term hardware. Concretely, Fig. 4 shows that when CNOT error rates are (realistically) between 1 and 10%, using SV is beneficial. The improvement from applying SV increases with QAOA depth, which is consistent with our analysis in Section III. Moreover, for higher qubit counts, the error rates required for obtaining improvement from SV are lower. The reason is the cost of applying N CNOT gates during the parity check, which grows with the number of nodes.

VI. EXPERIMENTS ON IONQ HARDWARE FOR SMALL N

To verify the results obtained in simulation, we tested error mitigation using our symmetry verification approach on an 11-qubit IonQ trapped-ion quantum computer [32] with an all-to-all connectivity. Each qubit register consists of a chain of spatially confined $^{171}\text{Yb}^+$ ions where the quantum states are encoded into the hyperfine sublevels of the atom.

We ran experiments using all nonisomorphic graphs on 3 and 4 nodes with the QAOA depth being 1, 2, or 3. The results are shown in Fig. 5. We observe improvement in the QAOA objective for most graphs and depths. The change in the approximation ratio from SV varies from a decrease of 4.5% to an improvement of 19.2%, with a mean improvement of 4.3%. The results observed on hardware align well with numerical simulations, since typical two-qubit gate error rates reported for IonQ trapped-ion systems are between 1% and 3%, matching the error rates for which our simulation experiments predicted improvement from SV.

We need to put into perspective the improvement in approximation ratio observed on IonQ hardware (up to 19.2%) and in numerical simulations with local noise (up to 3.4%). For 3-regular graphs, Farhi et al. [6] showed that using the QAOA ansatz, the approximation ratio at depth $d = 1$ must be no less than 0.692, and Wurtz et al. [7] showed an improved bound of 0.7559 for $d = 2$. Assuming a conjecture on the graphs that are the worst case (with no “visible” cycles), Wurtz et al. [7] also extended this bound to 0.7924 for $d = 3$. The best-known classical algorithm by Goemans and Williamson [33] lower bounds the approximation ratios by 0.8786 [34]. At the same time, it is known that MaxCut is NP-hard to approximate better than $\frac{16}{17} \approx 0.941$ in the worst case [35]. Therefore, a small (i.e., less than 10%) improvement in the approximation ratio can be essential to achieving quantum advantage.

VII. DISCUSSION

In the absence of full fault tolerance, error mitigation is required for the application of QAOA in practice. In this paper we demonstrate that symmetry verification applied to QAOA circuits improves the fidelity of the quantum state. We provide techniques for studying the scaling of error mitigation techniques with circuit size and depth. We use these techniques to demonstrate the scaling of symmetry verification for QAOA applied to MaxCut under local noise. Such scaling analysis is essential for the long-term goal of optimizing the use of error mitigation strategies. The methods we use in this work can be easily adapted to develop a similar understanding of error mitigation by symmetry verification in other classes of variational quantum algorithms, including the variational quantum eigensolver [36] and quantum alternating operator ansatz [37]. For these algorithms, the symmetries include particle number conservation and local particle number conservation.

Our analysis of local noise models suggests that verifying the bit-flip (\mathbb{Z}_2) symmetry of the cost function is useful when running QAOA circuits at higher depths. Because worst-case upper bounds on performance associated with QAOA become competitive with classical algorithms only at high depths,

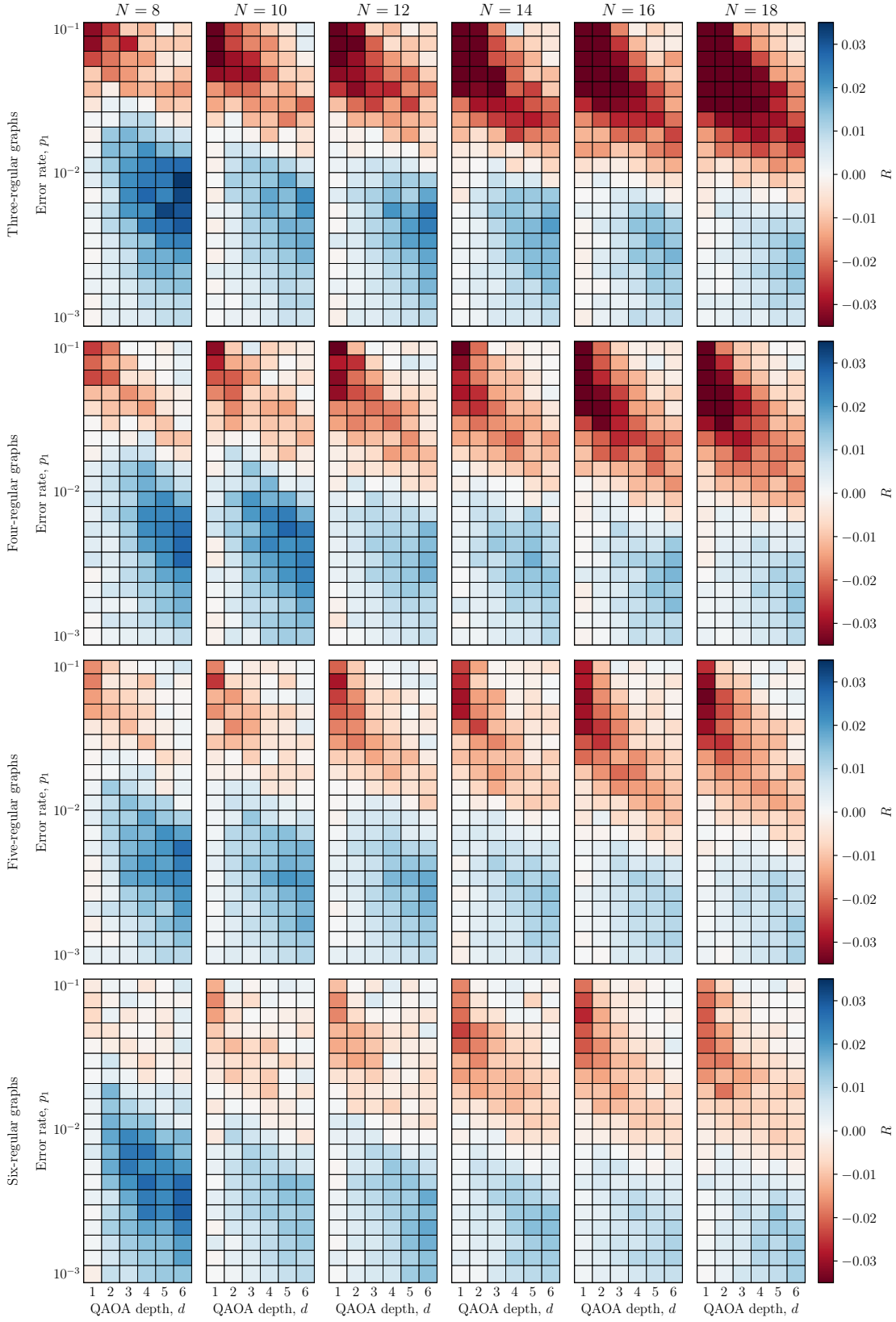


Fig. 4: Improvement in approximation ratio R given by Equation (33) for varying number of nodes N , QAOA depth d , and error rate p_1 . We see a greater improvement in R from the application of SV for larger QAOA depth. For larger qubit count N , lower single-qubit error rates are required in order to see an improvement in QAOA objective.

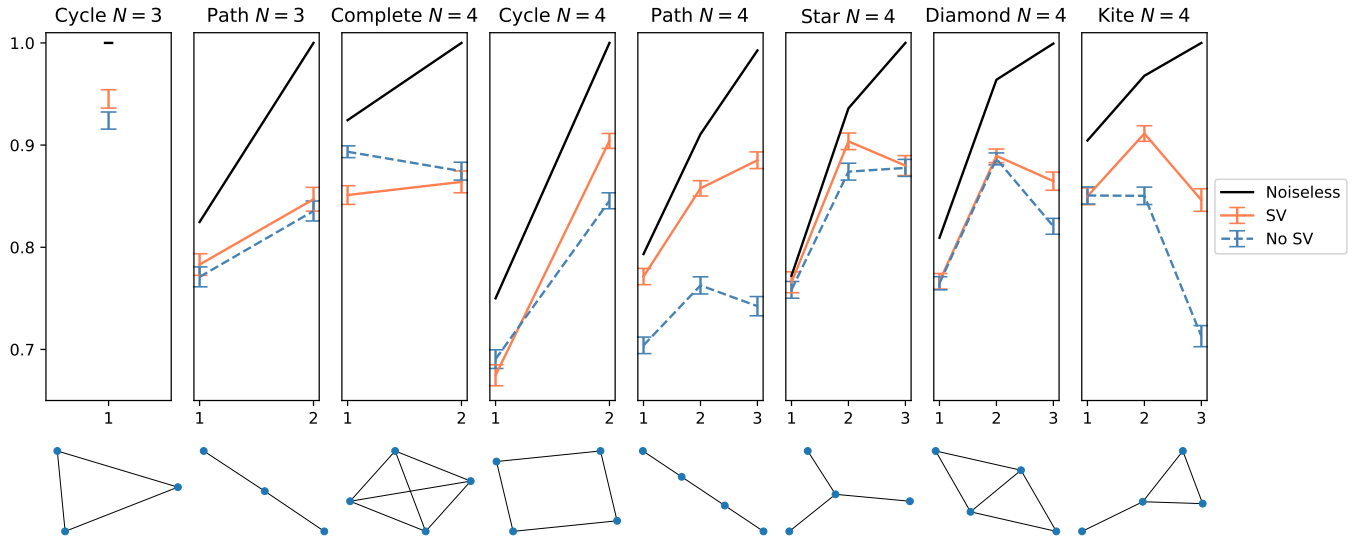


Fig. 5: Results of experiments done on trapped-ion quantum hardware made accessible by IonQ. We plot the approximation ratio after applying SV to QAOA applied to MaxCut (shown in orange), without applying SV (shown in blue), and noiseless simulation (shown in black). We observe an improvement after applying SV in all instances except Complete $N = 4$.

SV may become a useful part of the error mitigation stack of algorithms. We perform a set of numerical experiments to simulate the effects of the infidelity of two-qubit gates. These allow us to map out the parameter space where SV is expected to be useful. Our analysis via local error models indicates that higher-depth circuits show a greater increase in the fidelity of the final state. Experiments on IonQ hardware validate these findings. We also observe that verifying this bit-flip symmetry is more efficient than verifying permutation symmetries of the cost function. This result is consistent with the experimental evidence from superconducting IBM quantum processors reported in [22].

As a part of our analysis, we made use of the binary symplectic representation commonly used to describe quantum error-correcting codes. An interesting future direction is to use this representation to appropriately modify the mixer Hamiltonian B such that B and H are generators of a code subspace with a distance no less than 2. Then, one could perform parity checks that would detect all single-qubit errors and extend the reach of this analysis.

An important generalization to point out is Max- k -Cut, the problem of finding an approximate k -vertex coloring of a graph. Bravyi et al. [38] studied the approximation ratio achieved by QAOA for Max- k -Cut and compared it with the best-known classical approximation algorithms. The global symmetries of this model are permutations S_k . We expect that verifying this larger symmetry after the circuit has been executed will allow us to detect more errors and hence provide a greater boost in the fidelity.

ACKNOWLEDGMENT

This material is based upon work supported by the U.S. Department of Energy, Office of Science, National Quantum

Information Science Research Centers, the Office of Advanced Scientific Computing Research, Accelerated Research for Quantum Computing program, and Laboratory Directed Research and Development (LDRD) funding from Argonne National Laboratory, provided by the Director, Office of Science, at the U.S. Department of Energy under contract number DE-AC02-06CH11357. We gratefully acknowledge the computing resources provided on Bebop, a high-performance computing cluster operated by the Laboratory Computing Resource Center at Argonne National Laboratory.

REFERENCES

- [1] J. Preskill, “Quantum computing in the NISQ era and beyond,” *Quantum*, vol. 2, p. 79, 2018. [Online]. Available: <http://doi.org/10.22331/q-2018-08-06-79>
- [2] IBM, 2020. [Online]. Available: <https://research.ibm.com/blog/ibm-quantum-roadmap>
- [3] F. Arute *et al.*, “Quantum supremacy using a programmable superconducting processor,” *Nature*, vol. 574, no. 7779, pp. 505–510, 2019. [Online]. Available: <https://doi.org/10.1038/s41586-019-1666-5>
- [4] Y. Wu *et al.*, “Strong quantum computational advantage using a superconducting quantum processor,” *Physical Review Letters*, vol. 127, no. 18, 2021. [Online]. Available: <https://doi.org/10.1103/physrevlett.127.180501>
- [5] J. Preskill, “Fault-tolerant quantum computation,” 1997. [Online]. Available: <https://arxiv.org/abs/quant-ph/9712048>
- [6] E. Farhi, J. Goldstone, and S. Gutmann, “A quantum approximate optimization algorithm,” 2014. [Online]. Available: <https://arxiv.org/abs/1411.4028>
- [7] J. Wurtz and P. Love, “MaxCut quantum approximate optimization algorithm performance guarantees for $p \leq 1$,” *Physical Review A*, vol. 103, no. 4, 2021. [Online]. Available: <http://doi.org/10.1103/PhysRevA.103.042612>
- [8] J. Wurtz and D. Lykov, “Fixed-angle conjectures for the quantum approximate optimization algorithm on regular MaxCut graphs,” *Physical Review A*, vol. 104, no. 5, 2021. [Online]. Available: <https://doi.org/10.1103/physreva.104.052419>
- [9] J. Basso, E. Farhi, K. Marwaha, B. Villalonga, and L. Zhou, “The quantum approximate optimization algorithm at high depth for MaxCut

on large-girth regular graphs and the Sherrington–Kirkpatrick model,” 2021. [Online]. Available: <https://arxiv.org/abs/2110.14206>

[10] D. S. França and R. García-Patrón, “Limitations of optimization algorithms on noisy quantum devices,” *Nature Physics*, vol. 17, no. 11, pp. 1221–1227, 2021. [Online]. Available: <https://doi.org/10.1038/s41567-021-01356-3>

[11] C. Xue, Z.-Y. Chen, Y.-C. Wu, and G.-P. Guo, “Effects of quantum noise on quantum approximate optimization algorithm,” 2019. [Online]. Available: <https://arxiv.org/abs/1909.02196>

[12] J. Marshall, F. Wudarski, S. Hadfield, and T. Hogg, “Characterizing local noise in QAOA circuits,” *IOP SciNotes*, vol. 1, no. 2, p. 025208, 2020. [Online]. Available: <http://doi.org/10.1088/2633-1357/abb0d7>

[13] S. Wang *et al.*, “Noise-induced barren plateaus in variational quantum algorithms,” *Nature Communications*, vol. 12, no. 1, p. 6961, 2021. [Online]. Available: <http://doi.org/10.1038/s41467-021-27045-6>

[14] S. Endo, Z. Cai, S. C. Benjamin, and X. Yuan, “Hybrid quantum-classical algorithms and quantum error mitigation,” *Journal of the Physical Society of Japan*, vol. 90, no. 3, p. 032001, 2021. [Online]. Available: <http://doi.org/10.7566/JPSJ.90.032001>

[15] K. Temme, S. Bravyi, and J. M. Gambetta, “Error mitigation for short-depth quantum circuits,” *Physical Review Letters*, vol. 119, no. 18, 2017. [Online]. Available: <http://doi.org/10.1103/PhysRevLett.119.180509>

[16] T. Giurgica-Tiron, Y. Hindy, R. LaRose, A. Mari, and W. J. Zeng, “Digital zero noise extrapolation for quantum error mitigation,” *International Conference on Quantum Computing and Engineering*, 2020. [Online]. Available: <http://doi.org/10.1109/QCE49297.2020.00045>

[17] E. van den Berg, Z. K. Mineev, A. Kandala, and K. Temme, “Probabilistic error cancellation with sparse Pauli–Lindblad models on noisy quantum processors,” 2022. [Online]. Available: <https://arxiv.org/abs/2201.09866>

[18] A. Seif, Z.-P. Cian, S. Zhou, S. Chen, and L. Jiang, “Shadow distillation: Quantum error mitigation with classical shadows for near-term quantum processors,” 2022. [Online]. Available: <https://arxiv.org/abs/2203.07309>

[19] J. R. McClean, Z. Jiang, N. C. Rubin, R. Babbush, and H. Neven, “Decoding quantum errors with subspace expansions,” *Nature Communications*, vol. 11, no. 1, 2020. [Online]. Available: <http://doi.org/10.1038/s41467-020-14341-w>

[20] X. Bonet-Monroig, R. Sagastizabal, M. Singh, and T. E. O’Brien, “Low-cost error mitigation by symmetry verification,” *Physical Review A*, vol. 98, no. 6, p. 062339, 2018. [Online]. Available: <https://doi.org/10.1103/physreva.98.062339>

[21] R. Sagastizabal *et al.*, “Experimental error mitigation via symmetry verification in a variational quantum eigensolver,” *Physical Review A*, vol. 100, no. 1, 2019. [Online]. Available: <https://doi.org/10.1103/physreva.100.010302>

[22] R. Shaydulin, S. Hadfield, T. Hogg, and I. Safro, “Classical symmetries and the quantum approximate optimization algorithm,” *Quantum Information Processing*, vol. 20, no. 11, 2021. [Online]. Available: <https://doi.org/10.1007/s11128-021-03298-4>

[23] R. Shaydulin and A. Galdá, “Error mitigation for deep quantum optimization circuits by leveraging problem symmetries,” in *IEEE International Conference on Quantum Computing and Engineering*, 2021, pp. 291–300. [Online]. Available: <https://doi.org/10.1109/QCE52317.2021.00046>

[24] C. H. Papadimitriou and M. Yannakakis, “Optimization, approximation, and complexity classes,” *Journal of Computer and System Sciences*, vol. 43, no. 3, pp. 425–440, 1991. [Online]. Available: [https://doi.org/10.1016/0022-0000\(91\)90023-X](https://doi.org/10.1016/0022-0000(91)90023-X)

[25] M. A. Nielsen and I. L. Chuang, *Quantum Computation and Quantum Information*. Cambridge University Press, 2011. [Online]. Available: <https://doi.org/10.1017/CBO9780511976667>

[26] M. G. Davis *et al.*, “Towards optimal topology aware quantum circuit synthesis,” in *IEEE International Conference on Quantum Computing and Engineering*, 2020, pp. 223–234. [Online]. Available: <https://doi.org/10.1109/QCE49297.2020.00036>

[27] A. M. Childs and N. Wiebe, “Hamiltonian simulation using linear combinations of unitary operations,” *Quantum Information and Computation*, vol. 12, no. 11&12, pp. 901–924, 2012. [Online]. Available: <https://doi.org/10.26421/2Fqic12.11-12-1>

[28] J. R. McClean, Z. Jiang, N. C. Rubin, R. Babbush, and H. Neven, “Decoding quantum errors with subspace expansions,” *Nature Communications*, vol. 11, no. 1, p. 636, 2020. [Online]. Available: <https://doi.org/10.1038/s41467-020-14341-w>

[29] IBM, 2022. [Online]. Available: <https://quantum-computing.ibm.com>

[30] IonQ, 2022. [Online]. Available: <https://ionq.com/technology>

[31] R. Shaydulin, K. Marwaha, J. Wurtz, and P. C. Lotshaw, “QAOAKit: A toolkit for reproducible study, application, and verification of the QAOA,” in *International Workshop on Quantum Computing Software*. IEEE, 2021, pp. 64–71. [Online]. Available: <https://doi.org/10.1109/QCS54837.2021.00011>

[32] K. Wright *et al.*, “Benchmarking an 11-qubit quantum computer,” *Nature Communications*, vol. 10, no. 1, 2019. [Online]. Available: <http://doi.org/10.1038/s41467-019-13534-2>

[33] M. X. Goemans and D. P. Williamson, “Improved approximation algorithms for maximum cut and satisfiability problems using semidefinite programming,” *Journal of the ACM*, vol. 42, no. 6, pp. 1115–1145, 1995. [Online]. Available: <https://doi.org/10.1145/227683.227684>

[34] A. Frieze and M. Jerrum, “Improved approximation algorithms for MAX-CUT and MAX BISECTION,” *Algorithmica*, vol. 18, no. 1, pp. 67–81, 1997. [Online]. Available: <https://doi.org/10.1007/BF02523688>

[35] J. Håstad, “Some optimal inapproximability results,” *Journal of the ACM*, vol. 48, no. 4, pp. 798–859, 2001.

[36] A. Peruzzo *et al.*, “A variational eigenvalue solver on a photonic quantum processor,” *Nature Communications*, vol. 5, no. 1, 2014. [Online]. Available: <http://doi.org/10.1038/ncomms5213>

[37] M. Streif, M. Leib, F. Wudarski, E. Rieffel, and Z. Wang, “Quantum algorithms with local particle-number conservation: Noise effects and error correction,” *Physical Review A*, vol. 103, no. 4, 2021. [Online]. Available: <http://doi.org/10.1103/PhysRevA.103.042412>

[38] S. Bravyi, A. Kliesch, R. Koenig, and E. Tang, “Hybrid quantum-classical algorithms for approximate graph coloring,” 2020. [Online]. Available: <https://arxiv.org/abs/2011.13420>

APPENDIX A

$f(m)$ FOR DEPOLARIZING CHANNEL

Consider the case of even m . Because there are m errors, we first consider errors with $\vec{\alpha}$ having Hamming weight of i $\vec{\beta}$ having Hamming weight $m - i$. Note that i must be even because of the condition $\vec{\beta} \cdot \vec{1} \equiv 0 \pmod{2}$. There are $\binom{N}{m-i}$ ways of picking the vector $\vec{\beta}$. There are $\binom{N-m+i}{i} 2^{m-i}$ ways of choosing the vector in $\vec{\alpha}$ because it must have an entry 1 in at least $N - (m - i)$ positions (for the total number of errors to be m), which gives a factor of $\binom{N-m+i}{i}$. The vector $\vec{\alpha}$ can have 0 or 1 in the remaining $m - i$ positions, which gives a factor of 2^{m-i} . The full contribution to $f(m)$ takes the following form: For even m , doing this sum gives

$$\begin{aligned} f(m) &= \sum_{i \text{ even}}^m \binom{N}{m-i} 2^{m-i} \binom{N-m+i}{i} \\ &= \frac{1}{2} \binom{N}{m} (1 + 3^m). \end{aligned}$$

For odd m , the logic is the same as before except that we must consider errors for which $\vec{\beta}$ has a Hamming weight of $m - i$, where i is odd to satisfy the constraint $\vec{\beta} \cdot \vec{1} \equiv 0 \pmod{2}$. The contribution to $f(m)$ takes the following form:

$$\begin{aligned} f(m) &= \sum_{i \text{ odd}}^m \binom{N}{m-i} 2^{m-i} \binom{N-m+i}{i} \\ &= \frac{1}{2} \binom{N}{m} (-1 + 3^m). \end{aligned}$$

The submitted manuscript has been created by UChicago Argonne, LLC, Operator of Argonne National Laboratory ("Argonne"). Argonne, a U.S. Department of Energy Office of Science laboratory, is operated under Contract No. DE-AC02-06CH11357. The U.S. Government retains for itself, and others acting on its behalf, a paid-up nonexclusive, irrevocable worldwide license in said article to reproduce, prepare derivative works, distribute copies to the public, and perform publicly and display publicly, by or on behalf of the Government. The Department of Energy will provide public access to these results of federally sponsored research in accordance with the DOE Public Access Plan <http://energy.gov/downloads/doe-public-access-plan>.